INSTITUTE OF PHYSICS PUBLISHING PHYSICS IN MEDICINE AND BIOLOGY

Phys. Med. Biol. **49** (2004) 5157–5170 PII: S0031-9155(04)84011-9

Dosimetric evaluation of MRI-based treatment planning for prostate cancer*

L Chen, R A Price Jr, T-B Nguyen, L Wang, J S Li, L Qin, M Ding, E Palacio, C-M Ma and A Pollack

Radiation Oncology Department, Fox Chase Cancer Center, Philadelphia, PA 19111, USA

E-mail: Lili.Chen@fccc.edu

Received 23 July 2004, in final form 23 September 2004
Published 29 October 2004
Online at stacks.iop.org/PMB/49/5157
doi:10.1088/0031-9155/49/22/010

Abstract

The purpose of this study is to evaluate the dosimetric accuracy of MRI-based treatment planning for prostate cancer using a commercial radiotherapy treatment planning system. Three-dimensional conformal plans for 15 prostate patients were generated using the AcQPlan system. For each patient, dose distributions were calculated using patient CT data with and without heterogeneity correction, and using patient MRI data without heterogeneity correction. MR images were post-processed using the gradient distortion correction (GDC) software. The distortion corrected MR images were fused to the corresponding CT for each patient for target and structure delineation. The femoral heads were delineated based on CT. Other anatomic structures relevant to the treatment (i.e., prostate, seminal vesicles, lymph notes, rectum and bladder) were delineated based on MRI. The external contours were drawn separately on CT and MRI. The same internal contours were used in the dose calculation using CT- and MRI-based geometries by directly transferring them between MRI and CT as needed. Treatment plans were evaluated based on maximum dose, isodose distributions and dose–volume histograms. The results confirm previous investigations that there is no clinically significant dose difference between CT-based prostate plans with and without heterogeneity correction. The difference in the target dose between CT- and MRI-based plans using homogeneous geometry was within 2.5%. Our results suggest that MRI-based treatment planning is suitable for radiotherapy of prostate cancer.

(Some figures in this article are in colour only in the electronic version)

* The materials in this paper have been presented in part at the San Diego 2003 AAPM.

1. Introduction

Radiation therapy is one of the most effective treatment modalities for prostate cancer. Many investigators have demonstrated that dose escalation with three-dimensional (3D) conformal radiation therapy (3DCRT) and recently intensity-modulated radiation therapy (IMRT) potentially increases the cure rate while keeping complication risk at a reasonable level (Zelefsky *et al* 1998, Hanks *et al* 1998, Hanks 1999, Pollack *et al* 1999, 2000, 2002, Yeoh *et al* 2003). As dose levels are increased, the precise knowledge of target location and size and the accuracy of dose delivery become crucial. Magnetic resonance imaging (MRI) provides superior image quality for soft-tissue delineation over computed tomography (CT) and is widely used for target and organ delineation in radiotherapy for treatment planning (Khoo *et al* 2000, Tanner *et al* 2000, Potter *et al* 1992). The prostate volume on CT appears to be about 40% larger than on MRI (Rasch *et al* 1999). These results were consistent with those reported by Krempien *et al* (2002). Debois *et al* (1999) showed that improved prostate and rectal volume delineation from MRI could lead to improvements both in target coverage and rectal sparing. As a result of improved soft-tissue delineation the utilization of MRI for treatment planning of prostate cancer is desirable. Studies have been carried out to explore the efficacy of the use of MRI for radiotherapy treatment planning (Beavis *et al* 1998, Mah *et al* 2002a, 2002b, Michiels *et al* 1994, Mizowaki *et al* 2000, Lee *et al* 2003).

However, several perceived disadvantages of using MRI for treatment planning dose calculation have precluded its widespread use in this area. These disadvantages include the lack of electron density information for accurate dose calculation and image distortion leading to geometrical inaccuracies. Currently, MR and CT image fusion with CT-based dose calculation is the gold standard for prostate treatment planning. Although MR-CT image fusion has been widely accepted as a practical approach for both accurate anatomical delineation (using MRI data) and dose calculation (using CT data) it would be ideal if MRI could be used alone for prostate treatment planning (i.e., MRI-based treatment planning). The fusion process introduces additional error since it is often difficult to coordinate the CT and MR images, and substantial differences in bladder and rectal filling may lead to significant discordance. Furthermore, MRI-based treatment planning will avoid redundant CT imaging sessions, which in turn will avoid unnecessary radiation exposure to the patient. It also saves patient, staff and machine time.

Regarding the lack of electron density information in MRI, many studies have shown that there is no clinically significant difference in dose calculation between homogeneous and heterogeneous geometry for the pelvic region (Ma *et al* 1999, 2000, Chen *et al* 2002, Yang *et al* 2004). It has been common practice to use homogeneous geometry in treatment planning dose calculation for prostate cancer both for conventional treatment and IMRT. Therefore, the lack of electron density information in MRI is not considered to be a significant problem in terms of treatment planning accuracy for prostate cancer. This assumption is carefully examined in this work to provide a basis for MRI-based dose calculation, in which all the internal organs and structures (including the target) are delineated on MRI and the dose calculation is performed on homogeneous geometry built from the patient external contour drawn on MRI.

It is clear that before MRI alone can be used for treatment planning any significant image distortions must be quantified and corrected. Image distortion arises from both system-related effects and object-induced effects. System-related distortion is a result of inhomogeneities in the main magnetic field and non-linearities in spatial encoding gradient field while object-induced effects are a result of both chemical shift and susceptibility effects due to the differences in the resonant frequency between fat and water and the magnetic field

distortions introduced at tissue–air interfaces. The chemical shift artefacts and susceptibility distortion are larger on high-field MR units than on lower field MR units. While chemical shift artefacts and susceptibility distortion can cause significant spatial misregistrations at high fields, their impact on MRI at lower fields is substantially reduced. For fields below about 0.5 Tesla (T), imaging sequences that provide a sufficient signal-to-noise ratio keep geometric distortion due to either of these object-related effects below 1–2 pixels. This is achieved by defining a lower limit for the bandwidth of the readout gradient during image acquisition. One *in vivo* study has shown that with 0.2 T using a bandwidth readout gradient >100 Hz/pixel in frequency direction there is no artefact detected (Fransson *et al* 2001). In our clinical routine MR simulation, we have chosen 154 Hz/pixel in the frequency encoding direction, therefore the effects caused by chemical and susceptibility are considered negligible. For system-related distortions, different image distortion correction methods have been developed (Finnigan *et al* 1997, Fransson *et al* 1998, Schad *et al* 1987, 1992, Schubert *et al* 1999). Mah *et al* (2002a) showed that with a gradient distortion correction (GDC) the distortions of the external contour from MRI were insignificant for 3DCRT of prostate cancer, based on the tissue-maximum ratio (TMR) analysis using a 0.23 T open system and a 1.5 T closed system.

The objective of the current investigation is to directly compare the dosimetric accuracy of CT- and MRI-based treatment planning for prostate cancer for 15 patients using a commercially available treatment planning system—the AcQPlan system. We verify the assumption of the use of homogeneous geometry for dose calculation for prostate by comparing 3DCRT plans using CT-based dose calculation with and without heterogeneity correction. We quantify the residual MRI distortions with the use of the GDC software and examine their effect on the determination of external contours and dose distributions. The use of MRI-based digitally reconstructed radiographs (DRRs) for patient set-up is also discussed.

2. Materials and methods

2.1. The MRI scanner

A 0.23 T open MRI scanner (Philips Medical Systems, Cleveland, OH) was used for this study. The MR scanner consists of two poles of approximately 1 m diameter each. The separation between the two poles is 47 cm. The MR scan table can be moved in orthogonal planes along a set of rails mounted on the floor and on an orthogonal set of rails built in the couch. A flat table top made of special material, which is stiff and light, was inserted beneath the patient. A set of pads made of special foam was used to adjust the table height according to the patient size. The three triangulation lasers (centre and laterals) identical to those used on linear accelerators were used for patient positioning.

2.2. CT imaging procedure

All the patients were required to have a full bladder and were scanned in a supine position in a customized alpha cradle with knee support and a foot holder. Patients were scanned on a CT simulator (PICKER PQ 5000, Philips Medical Systems, Cleveland, OH) with a field of view (FOV) of 480 mm, matrix 512×512 (resolution 0.94 mm) and slice thickness 3 mm. The axial CT slices extended from the third lumbar vertebrae to the middle of the femurs. Three steel ball fiducials (1 mm in diameter) were used (one anterior and two laterals) on the skin surface to mark the centre of the prostate as an isocentric slice. Then skin tattoos were aligned with the fiducial markers for daily treatment set-up. The CT data were transferred

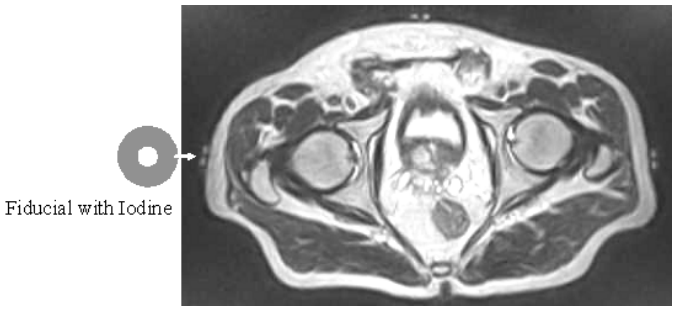

Figure 1. An MR image showing a special fiducial marker for MR localization. The outer diameter of the marker is 1.5 cm. The inner diameter is 4 mm. The grey part with iodine provides the MR signal. The hollow centre shows clearly on a single slice.

to the treatment planning workstation and the patient was transferred to the MRI room for scanning within 0.5 h post CT.

2.3. MR imaging procedure

Patients were scanned in a supine position in an alpha cradle with knee support and a foot holder (the same position as for CT). Three donut shaped fiducials (figure 1) were superimposed on the tattoos that mark the centre of the prostate as indicated by CT. A series of 48 axial slices (3 mm thickness) covering the whole pelvis based on the guidance image were acquired using turbo pin echo, 3D sequence, TR/TE 3000/140 ms, FOV 45–50 cm (depending on patients' anatomical dimensions), matrix 256 $\times$ 256, echo train length (ETL) 32, flip angle 90°, slice thickness 3 mm, number of excitations (NEX) 1, bandwidth (BW) 39.5 kHz, frequency direction horizontal and 9 min scan time. The MR images were post-processed for image distortion correction using the GDC software provided by the vendor. The distortion corrected MR images were transferred to the treatment planning workstation.

2.4. Target and structure delineation

In our institution (FCCC), CT–MR fusion with CT-based dose calculation has been a routine procedure for all prostate cancer patients. Each patient underwent a CT and an MR scan as part of a routine simulation procedure. CT images were loaded as primary images and MR images were loaded as secondary images and then fused to the CT images using the software available in the AcQSim system. Fifteen patients were included in this study. The femoral heads were contoured based on CT and the targets and other critical structures were contoured based on MRI. The external contours were determined separately based on CT and MRI to define patient geometry for dose calculation. The same internal contours were used in both CT-based and MRI-based dose calculation. The differences in internal structure volumes between CT and MRI were studied, which were a result of contour transfer between image modalities due to the difference in the pixel size between CT and MRI. It was considered to be more reliable to use the same set of internal structure contours for the plan comparison than using a new set of contours generated on MRI since this would introduce additional uncertainties in the contours between MRI and CT. Although the CT and MRI scans were performed within a small time interval ($<1/2$ h) the difference in the rectal and bladder fillings could affect the volumes of these organs significantly.

2.5. Measurement of residual MR image distortion after GDC

In order to study the effect of residual MRI distortion on the dosimetric accuracy of MRI-based treatment planning, the patient dimensions in both anterior/posterior (AP) and lateral (LAT) directions were measured on MRI (after GDC) and compared with those measured on distortion-free CT images. The differences of the external contours between CT and MRI on the treatment isocentric slice were measured to estimate the error of residual MRI distortion. The values determined this way should have included the residual MRI distortions (both system related and object induced), differences in external contours due to patient set-up between CT and MRI simulation, and the errors introduced by image fusion, which was estimated to be at the 2–3 mm level, which was achieved routinely in our clinic. There were rejections occasionally, as determined by the treating physician, when significant differences were found in some internal structures due to large changes in the rectal and bladder fillings between CT and MRI but this was not the case for the 15 patients investigated in this work.

2.6. Dose calculations and evaluations

The AcQPlan system version 5 was used for the study, which is capable of performing dose calculation on both CT and MRI. A four-field 3D conformal planning technique was used for the study. First, we verified the dosimetry accuracy of using homogeneous geometry for prostate planning. This was done by calculating dose distributions using the distortion-free CT data with and without heterogeneity correction (equivalent TAR), respectively. As a result, two treatment plans were generated for each patient with the same treatment parameters (i.e., energy, gantry angle, block shape and size, and dose prescription). We used 10 or 18 MV photon beams with an 8 mm block margin around the planning target volume (PTV). Second, we evaluated the dosimetry accuracy of CT-based and MRI-based dose calculation. This was achieved by calculating dose distributions using both CT and MRI data without heterogeneity correction (i.e., using homogeneous geometry defined by the patient external contour). The same MUs obtained from CT-based plans were directly used in MRI-based plans so that the effects of residual MRI distortions on external contours and the differences in internal structure volumes between CT and MRI can be quantified. The plans were evaluated based on isodose distributions and dose–volume histograms (DVHs) for the target and the critical structures. Based on the DVHs, doses were reported at 95% of the planned treatment volume (PTV), D95, for the prostate, at 35% (D35) and 17% (D17) of the rectum volume, and at 50% (D50) and 25% (D25) of the bladder volume. These dose points were chosen based on our current clinical acceptance criteria for prostate cancer treatments.

3. Results and discussion

3.1. Measurement of residual MRI distortion and external contour

The GDC software improves MR image distortion significantly in the peripheral regions of the FOV, which is important to the accurate determination of patient external contours for MRI-based treatment planning. Figure 2 shows an example of the MR images before and after the gradient distortion correction. The effect of MR distortion on external contours was reduced significantly after the GDC. Similar improvement was observed for all patients investigated.

The residual distortions after the GDC along the major axes on the treatment isocentric slice were related to the patient anatomic size. Table 1 summarizes our results for 15 patients. As distortion increases with the distance between the magnetic isocentre and the point of

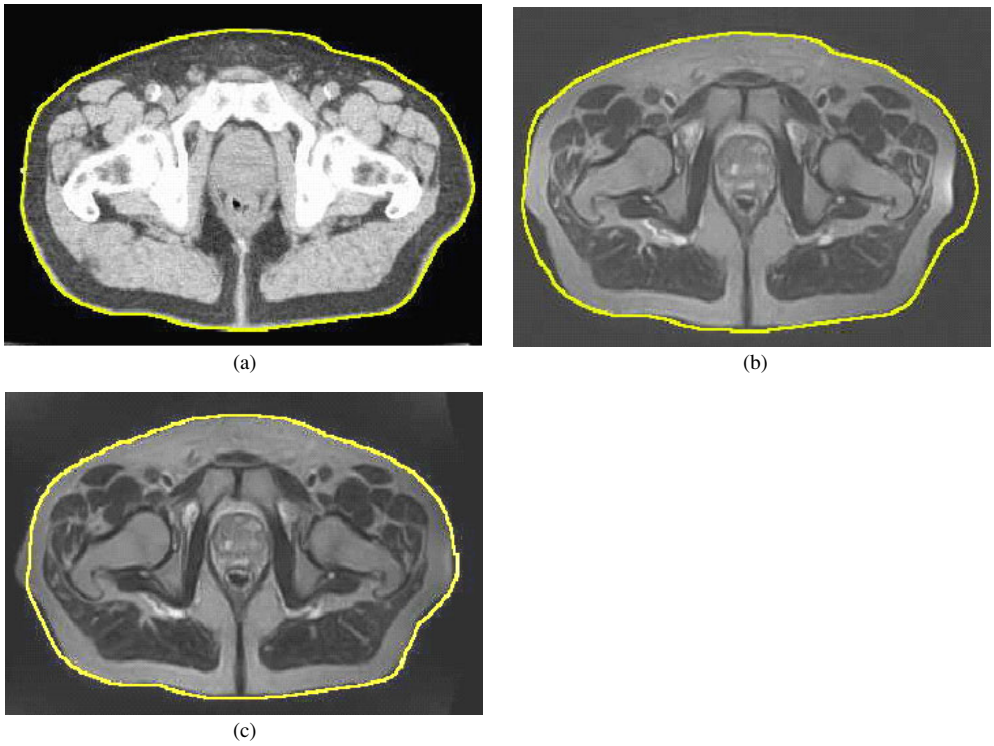

Figure 2. Comparison of CT and MR images for a prostate patient: (a) a distortion-free CT image, (b) an MR image before the GDC and (c) an MR image after the GDC.

interest, the distortion becomes significant when patient size is greater than a certain value. Our results showed that in the AP (anterior and posterior) dimension all measurements were less than 30 cm and there were no significant distortions in this direction. For the LAT (lateral) dimensions, the residual distortion was negligible (range 0–0.2 cm) for patient sizes less than 36 cm (see patients 10 and 14). For patient sizes between 36 and 38 cm (patients 2, 4, 9 and 11) the maximum distortion was 0.7 cm (range 0–0.7 cm). For patient sizes between 38.5–40 cm (patients 3, 12, 13 and 15) the maximum distortion was 1.0 cm (range 0.2–1.0 cm). For patient sizes larger than 40 cm (patients 1, 5, 6 and 8) the maximum distortion was 2.7 cm (range 0.3–2.7 cm). The exact reason for the large residual distortion at the peripheral regions was not found. There may be several possibilities. A major possibility was the difference between the theoretical magnetic field distribution calculated by the GDC software and the actual field distribution. Without knowing the actual gradient distortion accurately in the peripheral regions the GDC cannot make a perfect correction. A minor possibility was the combination of the large distortion and the limited FOV (45–50 cm). For patients greater than 40 cm (e.g., patients 1, 5 and 6 in table 1 are greater than 44 cm in lateral dimensions) part of the patient geometry may be outside the FOV due to MR distortion. This part of the geometry will not be recovered by the GDC software although physically it is within the FOV. It should be mentioned that the residual distortions shown in table 1 also included the changes in patient dimensions between CT and MRI simulation due to patient set-up and the error introduced by image fusion.

Our results are consistent with previous studies. Beavis *et al* (1998) reported maximum distortion errors of ± 1 mm for a 10 cm FOV and ± 2 mm for a 24 cm FOV. These results were

Table 1. Patient dimensions measured on CT (distortion free) and the residual distortions on MR calculated as the difference between external contour points along the major axes on the isocentric slice on CT and those on MRI.

	Dimension on CT (cm)		Residual distortion (cm)			
Patient no	A/P	R/L	Anterior	Posterior	Right	Left
1	28.0	45.4	0.0	0.0	2.7	1.7
2	21.0	38.0	0.0	0.0	0.0	0.6
3	22.5	38.8	0.0	0.0	0.8	0.7
4	21.5	36.7	0.0	0.0	0.0	0.0
5	26.0	44.1	0.0	0.0	1.1	1.6
6	25.9	44.5	0.4	0.4	2.2	0.7
7	21.8	37.0	0.0	0.0	0.7	0.0
8	26.6	43.0	0.0	0.3	1.4	0.3
9	22.0	36.4	0.0	0.2	0.5	0.0
10	19.1	34.3	0.0	0.0	0.0	0.0
11	20.6	37.0	0.0	0.2	0.5	0.3
12	21.8	39.3	0.0	0.0	0.8	0.2
13	25	39.9	0.0	0.0	1.0	0.5
14	21	34.6	0.0	0.0	0.0	0.2
15	24	38.5	0.0	0.0	0.7	0.8

similar to those reported by other investigators (Hill *et al* 1994, Mizowaki *et al* 2000). Our previous study (Mah *et al* 2002a) estimated that the effect of image distortion was clinically insignificant for the prostate targets and nearby critical structures; they were all within 15 cm of the isocentre and the distortion error was found to be less than 2 mm on our low-field MR unit. The effect of residual image distribution on dose calculation (e.g., the effect on DVH calculation) was considered to be negligible after the GDC. In fact, we expect that MRI-based treatment planning will result in more accurate DVH calculation because soft-tissue structures can be more accurately delineated on MRI due to its superior soft-tissue contrast and the elimination of errors in patient set-up between CT and MR scans and in image fusion. The distortion error is more pronounced for the external contours and its effect can be clinically significant since the external contours will define the homogenous patient geometry (and the beam paths). The uncertainty in the fiducial locations will also affect the determination of the isocentre. To ensure the accuracy of MRI-based treatment planning and its clinical implementation we have set a criterion for patient selection with maximum lateral dimensions less than 38 cm. For patient lateral sizes larger than 38 cm we still use the standard CT and MR fusion technique with CT-based dose calculation. Approximate 90% patients in our clinic have lateral dimensions less than 38 cm based on a separated study.

3.2. Measurement of internal structure volumes

Table 2 shows the volume differences between CT and MRI for the prostate targets, seminal vesicles (SV) and critical structures as measured on the AcQSim. These differences were introduced by the contour transfer process and were thought mainly due to the difference in image pixel size between CT (512 $\times$ 512 matrix) and MRI (256 $\times$ 256 matrix). Similar small differences were also observed when patient plans were transferred from the AcQSim to other treatment planning systems. For structures with a relatively small volume, such differences may have noticeable effects on the DVH comparison between MRI- and CT-based dose calculation (see section 3.4). However, this will no longer be a problem when both contouring and treatment planning are performed on MRI directly.

Table 2. Internal structure volumes measured on MRI and CT as reported by the AcQPlan system. The internal contours were directly transferred between MRI and CT.

	GTV (cm^3)		SV (cm^3)		Rectum (cm^3)		Bladder (cm^3)	
Patient no	MR	CT	MR	CT	MR	CT	MR	CT
1	36.8	34.6	6.1	5.8	101.5	95.0	97.5	92.6
2	36.7	34.4	N/A	N/A	84.4	78.5	129.1	123.9
3	65.0	62.3	N/A	N/A	52.3	48.2	128.7	124.9
4	60.1	57.1	12.7	12.0	75.3	70.7	81.0	77.8
5	97.8	94.4	16.9	16.3	125.9	120.4	68.5	65.4
6	140.0	134.4	6.2	6.0	101.5	95.2	121.0	115.8
7	70.9	67.4	5.9	5.5	58.2	53.0	175.1	168.1
8	67.3	64.6	9.1	8.6	47.4	46.1	201.4	194.9
9	58.7	56.0	5.0	4.9	60.4	56.0	284.0	274.8
10	48.5	46.3	11.0	10.5	54.9	51.6	216.4	210.8
11	33.1	31.2	6.2	6.0	41.3	38.2	60.7	58.1
12	31.9	30.4	3.1	3.1	67.3	63.8	168.5	165.0
13	38.1	36.8	5.0	4.9	59.2	54.9	172.7	168.4
14	63.5	61.8	12.6	12.0	55.3	51.4	91.9	90.1
15	70.2	67.6	9.9	9.4	55.4	51.2	106.6	103.7

Table 3. The per cent dose difference between CT plans calculated with and without heterogeneity correction (expressed as dose without correction minus dose with correction divided by the prescription dose).

Patient no	Max dose	D95 prostate	D17 rectum	D35 rectum	D25 bladder	D50 bladder
1	0.75	0.50	0.95	0.70	0.75	0.45
2	0.80	0.00	0.75	1.15	0.25	0.00
3	0.95	0.75	0.75	0.70	0.70	0.25
4	0.55	0.50	0.45	0.70	0.95	0.75
5	2.50	0.45	0.95	1.20	1.40	1.70
6	0.70	0.45	0.75	1.20	0.70	0.95
7	0.65	0.25	0.50	0.70	0.70	0.70
8	2.35	1.40	1.45	1.40	1.20	0.25
9	0.30	0.25	1.20	1.20	0.70	0.45
10	1.25	0.95	0.70	1.40	0.70	0.25
11	1.70	0.25	1.00	1.00	1.00	0.75
12	2.60	0.40	1.50	1.40	0.65	0.05
13	0.50	0.00	0.70	0.95	0.95	0.00
14	0.75	0.70	0.95	0.95	1.20	0.95
15	2.45	1.20	2.40	1.70	2.60	2.65
Mean ± SD	1.25 ± 0.83	0.54 ± 0.40	1.00 ± 0.49	1.09 ± 0.31	0.96 ± 0.53	0.66 ± 0.71

3.3. Dosimetric verification of prostate planning using homogeneous geometry

To verify the dosimetry accuracy of prostate treatment planning using homogeneous patient geometry, we have performed dose calculations on CT with and without heterogeneity correction. The difference in the isocentre dose (prescription point) using the same MUs for the two plans was within 2.6% for all the cases. This is equivalent to a 2.6% difference in the MUs used for the treatment if the same dose is prescribed at the isocentre. We also examined the volumetric dose differences between these plans. Table 3 summarizes the results of CT-based plans with and without heterogeneity correction for maximum dose, D95 for the

prostate target, D17 and D35 for the rectum, and D25 and D50 for the bladder. It shows clearly that the differences in maximum doses and all other dose parameters are clinically insignificant (<2.6% of the prescription dose). The mean values averaged over 15 patients for maximum doses, D95 for the prostate, D17 and D35 for the rectum, and D25 and D50 for the bladder are $1.25 \pm 0.83\%$, $0.54 \pm 0.4\%$, $1.0 \pm 0.49\%$, $1.09 \pm 0.31\%$, $0.96 \pm 0.53\%$ and $0.66 \pm 0.71\%$ of the prescribed target dose, respectively. Our results confirmed previous observations that the dose with heterogeneity correction is slightly lower than that without it because of the additional attenuation from the bones but it has no clinical significance for 3DCRT and IMRT dose calculation for the pelvic region (Ma *et al* 1999, 2000, Chen *et al* 2002, Yang *et al* 2004). However, the above results are useful in establishing a foundation for the dose comparison between CT- and MRI-based treatment planning using homogeneous geometry (see next section).

It has been common practice to use homogeneous geometry for prostate treatment planning. This is not only supported by the sufficient dosimetry accuracy as discussed above but also by other practical considerations in using homogeneous geometry for dose calculation in the pelvic region. One consideration is the use of contrast agents for imaging that sometimes changes the CT numbers in the bladder significantly. Unless one modifies these CT numbers manually, a significant change in the electron density of the bladder will occur and the target and other organ doses will be affected significantly if one applies heterogeneity correction. Another consideration is the occasional occurrence of large gas pockets in the rectum on the planning CT, which may affect the dose distribution and/or MU calculation significantly when heterogeneity correction is used. These gas pockets often show up briefly during imaging and treatment for some patients but have little effect on the treatment in reality. The use of homogeneous geometry will avoid this problem and provide more accurate dose calculation for the treatment. Furthermore, the use of homogeneous geometry for dosimetric evaluation of CT- and MRI-based dose calculation also eliminates the possibility of any dose differences caused by the particular dose calculation algorithm used.

3.4. Dosimetric evaluation of CT- and MR-based treatment plans

Based on the results described above, it is reasonable to evaluate the dosimetric accuracy of CT- and MRI-based treatment planning using homogeneous geometry following our clinical practice. Figure 3 shows the isodose distributions and DVHs for an MRI-based plan and a CT-based plan. It can be seen that the differences in both isodose distributions and DVHs between the two plans are not clinically significant. Similar agreement was found between the plans for the rest of the patients investigated. The difference in the isocentre dose (prescription point) for the two plans was within 2% for all cases. The volumetric dose difference between MRI-based planning and CT-based planning is summarized in table 4.

For all 15 patients investigated, the maximum difference is less than 1.5% in the maximum dose and less than 1% in D95 of the prostate between MR- and CT-based plans, indicating consistent dose calculation accuracy of CT- and MRI-based treatment planning. In general, the differences in the rectal D17 and D35 and the bladder D25 and D50 are within 4% of the prescription dose except for patient 1 and 12, who showed a -9.8% difference in rectal D35 and a -12.4% difference in bladder D25, respectively. Those discrepancies do not correlate with residual MRI distortions. As shown in table 1, large residual distortions (>1 cm) appeared for patients 1, 5, 6, 8 and 13 while larger dose discrepancies were found for patients 1 and 12. The residual MRI distortions should not affect the dose calculation significantly because most differences in the external contours along the beam incident directions were less than 1 cm. When multiple beams are used in a 3DCRT treatment, it is unlikely that a treatment plan will

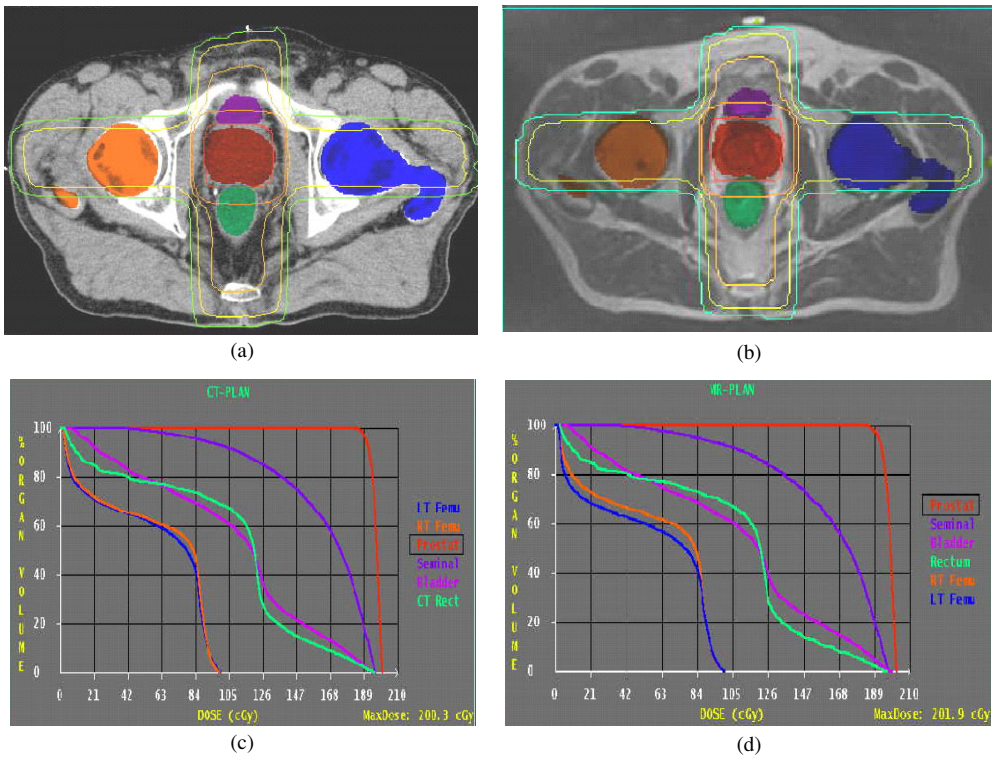

Figure 3. Comparison of isodose distributions based on CT (a) and MRI (b) and their corresponding DVHs for the PTV and critical structures based on CT (c) and MRI (d). The isodose lines represent 95%, 70%, 60%, 40% and 20% of the prescribed target dose.

Table 4. The per cent dose difference between MRI-based and CT-based plans calculated using homogeneous patient geometry (expressed as dose calculated on CT minus dose calculated on MRI divided by the prescription dose). The same monitor units derived from the CT plans were used for the dose calculation for the MRI-based plans.

Patient no	Max dose	D95 prostate	D17 rectum	D35 rectum	D25 bladder	D50 bladder
1	−0.60	−0.75	−0.25	−9.80	0.45	1.70
2	−1.50	−0.25	0.25	−0.70	−5.5	3.80
3	−0.05	0.00	−0.50	−0.50	0.00	0.50
4	−0.90	0.00	1.45	−0.25	−1.90	−0.50
5	−0.25	0.00	0.00	0.70	0.25	0.45
6	−0.45	−0.20	−0.50	−0.25	−0.45	0.00
7	−0.35	0.25	−1.45	−0.45	−0.20	0.00
8	−0.45	0.50	−0.70	−0.20	0.95	0.25
9	0.65	0.50	−0.50	0.00	−1.65	−3.30
10	0.10	0.25	0.70	−0.0	1.45	0.70
11	−0.25	0.25	−3.25	−1.00	0.75	0.25
12	0.50	0.25	0.00	0.00	−12.4	−1.90
13	−0.60	0.00	−1.20	0.00	1.90	0.75
14	−0.80	−0.25	2.15	0.75	−0.95	0.20
15	−0.25	0.00	−2.40	−0.20	1.20	1.15
Mean ± SD	−0.35 ± 0.54	0.04 ± 0.32	−0.41 ± 1.36	−0.81 ± 2.53	−1.07 ± 3.62	0.27 ± 1.56

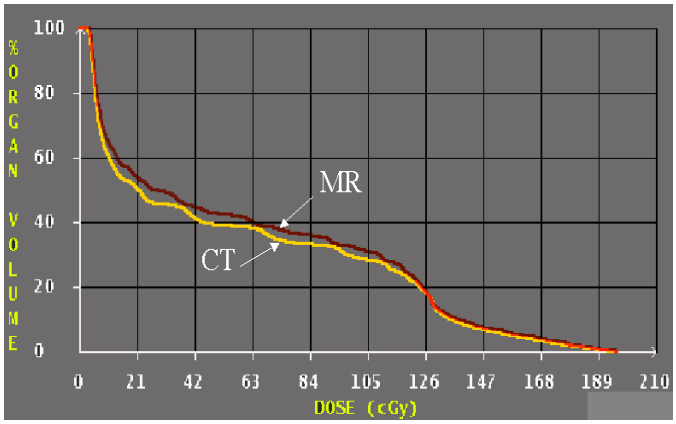

Figure 4. Comparison of DVHs for the rectum based on CT and MRI for patient 1. Since the DVH curves are 'flat' a small change in the rectal volume leads to a large change in the dose such as D35 but not in D17.

be affected significantly if only one or two beams are inaccurate by 1 cm in equivalent path length.

The large discrepancies for patient 1 and 12 are likely attributed to the differences in structure volumes between CT and MRI, which was mainly caused by the difference in pixel size between CT and MRI since we used the same internal contours and the contours were transferred directly from CT to MRI. These discrepancies also reflect the intrinsic uncertainty in contour determination using CT and/or MRI, which will not be a problem when only one image modality is used. A closer examination of the treatment plans for patients 1 and 12 reveals that the rectal and bladder DVH curves are very 'flat' at D35 and D25 for these two patients. The −9.8% difference in the rectal D35 corresponds to a 2.3% change in the rectal volume for patient 1 (see figure 4) and the −12.4% difference in the bladder D25 corresponds to a 4.7% change in the bladder volume for patient 12 (not shown). These are not unexpected because of the similar differences in the absolute volumes between CT and MRI for the two patients (see table 2).

A recent study by Lee *et al* (2003) also showed small differences in target and critical structure doses for five prostate cases planned separately using CT and MRI. The maximum difference was less than 3.2% in the maximum, minimum and mean target doses although the target volumes drawn on CT and MRI differed by more than 30% in some cases. This again indicated that accurate target delineation based on MRI will have a significant clinical impact for prostate treatment while dose calculation using homogeneous geometry based on MRI data is reasonable. They also investigated assigning a bulk density to the bones in MRI-based dose calculation and found the maximum dose difference was reduced marginally (from 3.2% to 2%). The maximum difference was 6.6% in the maximum rectal dose and 4.2% in the maximum bladder dose, respectively. The mean dose to the bladder and rectum was no longer meaningful due to the large differences in the rectum and bladder volumes (up to 500%) since there was no protocol to control the volumes between CT and MRI scans (possibly due to the large time intervals between the two scans).

3.5. MRI-based DRRs

CT-based DRRs are routinely used for patient treatment set-up verification by comparing with portal film or electronic portal imaging devices (EPID). However, MRI-derived DRRs do not

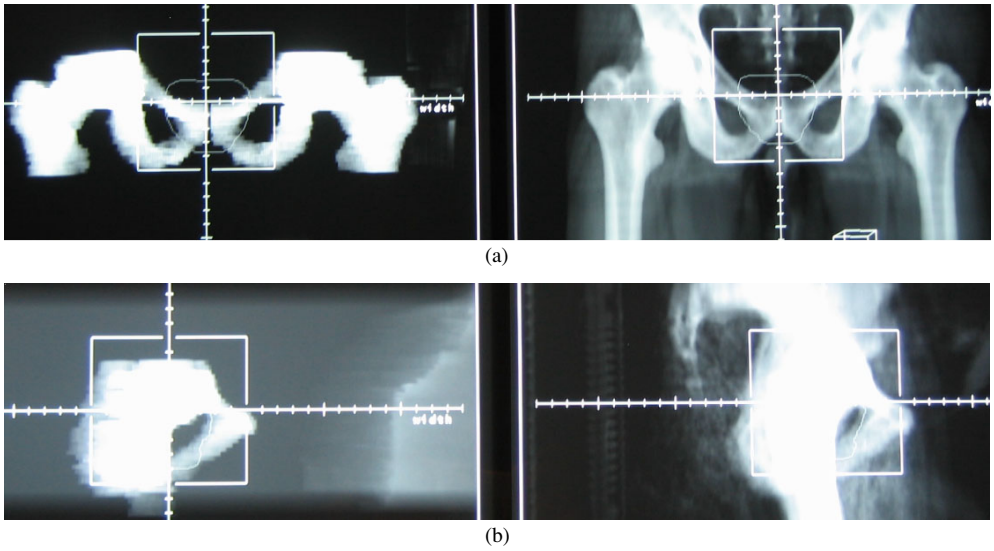

Figure 5. Comparison of MRI-based DRRs (left) and CT-based DRRs (right) for a prostate patient: (a) coronal view and (b) sagittal view.

provide enough bony structure information and therefore cannot be used directly for checking patient positions. To overcome this problem, a practical method to derive MRI-based DRRs for IMRT prostate patient set-up has been developed. The relevant bony structures on MRI including pubic symphysis, femoral heads and acetabulum are contoured and assigned a bulk density of 2.0 g cm^{-3}. The bony structures are then clearly shown on the MRI-derived DRRs and can be used for patient treatment set-up verification (figure 5). The accuracy of this method has been verified by comparing with CT-derived DRRs and the agreement between the two methods is estimated to be 2–3 mm based on 18 patients. At FCCC, we use an ultrasound target localization system (BAT, NOMOS, Sewickley, PA) for routine prostate treatment to improve patient set-up and target re-localization accuracy. MRI-derived internal contours actually provide better agreement with ultrasound images than CT-based contours and therefore result in better correction for prostate inter-faction motion. In our clinical implementation, MRI-based DRRs are used during initial treatment set-up together with BAT and later as a backup for the BAT system if a patient cannot be set up using BAT due to various reasons or if the BAT system is down.

4. Summary

The purpose of this study is to explore the use of MRI-based treatment planning for prostate cancer and to verify the dosimetry accuracy of its clinical implementation using a commercial treatment planning system. Our results confirm that treatment planning dose calculations using MRI-derived homogenous geometry are adequate for patient sizes within 38 cm after MR image distortion is corrected using the GDC software. MRI-derived DRRs utilizing the outlines of relevant bony structures are adequate for initial patient set-up. Further investigation of MRI-based treatment planning is being carried out for intensity-modulated radiation therapy of prostate cancer and other treatment sites.

Acknowledgments

This project was supported in part by grants from the DOD (PC030800) and the NIH (CA78331). We would also like to thank the support from Philips Medical Systems (Cleveland, OH), especially Dr Michael Steckner and David Abraham for their excellent technical assistance. We are indebted to Dr Gerald E Hanks for his foresight in initiating MRI-simulation at Fox Chase Cancer Center.

References

Beavis A W, Gibbs P, Dealey R A and Whitton V J 1998 Radiotherapy treatment planning of brain tumours using MRI alone *Br. J. Radiol.* **71** 544–8

Chen L, Li J, Mah D, Ma C-M, Wang L, Ding M, Freedman G, Movsas B and Pollack A 2002 Monte Carlo investigation of dosimetry accuracy for MR-based treatment planning *Med. Phys.* **29** 1339 (abstract)

Debois M *et al* 1999 The contribution of magnetic resonance imaging to the three-dimensional treatment planning of localized prostate cancer *Int. J. Radiat. Oncol. Biol. Phys.* **45** 857–65

Finnigan D J *et al* 1997 Distortion-corrected MR images for pelvic radiotherapy treatment planning *Proc. 19th L H Gray Conf.* chapter 3, pp 72–6

Fransson A, Andreo P and Potter R 2001 Aspects of MR image distortions in radiotherapy treatment planning. *Strahlenther. Onkol.* **177** 59–73

Fransson A *et al* 1998 System-specific geometric distortions in MR images from a 0.2 T resistive MRI unit *Radiother. Oncol.* **48** S187

Hanks G E 1999 Progress in 3D conformal radiation treatment of prostate cancer *Acta Oncol.* **38** 69–74

Hanks G E *et al* 1998 Dose escalation with 3D conformal treatment: five year outcomes, treatment optimization and future directions *Int. J. Radiat. Oncol. Biol. Phys.* **41** 501–10

Hill D L *et al* 1994 Accurate frameless registration of MR and CT images of the head: applications in planning surgery and radiation therapy *Radiology* **19** 447–54

Khoo V S, Adams E J, Saran F, Bedford J L, Perks J R, Warrington A P and Brada M 2000 A comparison of clinical target volumes determined by CT and MRI for the radiotherapy planning of base of skull meningiomas *Int. J. Radiat. Oncol. Biol. Phys.* **46** 1309–17

Krempien R C, Schubert K, Zierhut D, Steckner M C, Treiber M, Harms W, Mende U, Latz D, Wannenmacher M and Wenz F 2002 Open low-field magnetic resonance imaging in radiation therapy treatment planning *Int. J. Radiat. Oncol. Biol. Phys.* **53** 1350–60

Lee Y K, Bollet M, Charles-Edwards G, Flower M A, Leach M O, McNair H, Moore E, Rowbottom C and Webb S 2003 Radiotherapy treatment planning of prostate cancer using magnetic resonance imaging alone *Radiother. Oncol.* **66** 203–16

Ma C-M, Mok E, Kapur A, Findley F, Brain S, Forster F and Boyer A L 1999 Clinical implementation of a Monte Carlo treatment planning system *Med. Phys.* **26** 2133–43

Ma C-M, Pawlicki T, Jiang S B, Mok E, Kapur A, Xing L, Ma L and Boyer A L 2000 Monte Carlo verification of IMRT dose distributions from a commercial treatment planning optimization system. *Phys. Med. Biol.* **45** 2483–95

Mah D *et al* 2002a MRI Simulation: effect of gradient distortions on three-dimensional prostae cancer plans *Int. J. Radiat. Oncol. Biol. Phys.* **53** 757–65

Mah D, Steckner M, Palacio E, Mitra R, Richardson T and Hanks G E 2002b Characteristics and quality assurance of a dedicated open 0.23 T MRI for radiation therapy simulation *Med. Phys.* **29** 2541–7

Michiels J *et al* 1994 On the problem of geometric distortion in magnetic resonance images for stereotactic neurosurgery *Magn. Reson. Imaging* **12** 749–65

Mizowaki T, Nagata Y, Okajima K, Kokubo M, Negoro Y, Araki N and Hiraoka M 2000 Reproducibility of geometric distortion in magnetic resonance imaging based on phantom studies *Radiother. Oncol.* **57** 237–42

Pollack A, Zagars G K and Rosen I I 1999 Prostate cancer treatment with radiotherapy: maturing methods that minimize morbidity *Semin. Oncol.* **26** 150–61

Pollack A, Zagars G K, Smith L G, Lee J J, von Eschenbach A C, Antolak J A, Starkschall G and Rosen I 2000 Preliminary results of a randomized radiotherapy dose-escalation study comparing 70 Gy with 78 Gy for prostate cancer *J. Clin. Oncol.* **18** 3304–911

Pollack A, Zagars G K, Starkschall G, Antolak J A, Lee J J, Huang E, von Eschenbach A C, Kuban D A and Rosen I 2002 Prostate cancer radiation dose response: results of the M. D. Anderson phase III randomized trial *Int. J. Radiat. Oncol. Biol. Phys.* **53** 1097–105

Potter R, Heil B, Schneider L, Lenzen H, Al-Dandashi C and Schnepper E 1992 Sagittal and coronal planes from MRI for treatment planning in tumors of brain, head and neck: MRI assisted simulation *Radiother. Oncol*. **23** 127–30

Rasch C, Barillot I, Remeijer P, Touw A, van Herk M and Lebesque J V 1999 Definition of the prostate in CT and MRI: a multi-observer study *Int. J. Radiat. Oncol. Biol. Phys*. **43** 57–66

Schad L R *et al* 1992 Radiotherapy treatment planning of basal meningiomas: improved tumor localization by correlation of CT and MR imaging data *Radiother. Oncol*. **25** 56–62

Schad L *et al* 1987 Correction of spatial distortion in MR imaging: a prerequisite for accurate stereotaxy *J. Comput. Assist. Tomogr.* **11** 499–505

Schubert K *et al* 1999 Integration of an open magnetic resonance scanner in therapy simulation and three-dimensional radiation treatment planning *Strahlenther. Onkol*. **175** 225–31

Tanner S F, Finnigan D J, Khoo V S, Mayles P, Dearnaley D P and Leach M O 2000 Radiotherapy planning of the pelvis using distortion corrected MR images: the removal of system distortions *Phys. Med. Biol*. **45** 2117–32

Yang J, Li J, Chen L, Price R A, McNeeley S, Qin L, Wang L, Xiong W and Ma C-M 2004 Monte Carlo evaluation of heterogeneity effect in IMRT treatment planning for prostate cancer *Phys. Med. Biol*. at press

Yeoh E E K *et al* 2003 Evidence for efficacy without increased toxicity of hypofractionated radiotherapy for prostate carcinoma: early results of a Phase III randomized trial *Int. J. Radiat. Oncol. Biol. Phys*. **55** 943–55

Zelefsky M J *et al* 1998 Dose escalation with three-dimensional conformal radiation therapy affects the outcome in prostate cancer *Int. J. Radiat. Oncol. Biol. Phys*. **41** 491–500